PHYSICAL REVIEW B VOLUME 53, NUMBER 6 1 FEBRUARY 1996-II

Neutron-scattering study of the impulse approximation in ZrH_2

A. C. Evans* and D. N. Timms
Division of Physics, Portsmouth University, Park Building, King Henry I Street, Portsmouth PO1 2DZ, United Kingdom

J. Mayers and S. M. Bennington
Rutherford Appleton Laboratory, Chilton, Didcot, Oxfordshire OX11 0QX, United Kingdom

(Received 14 August 1995)

We report inelastic-neutron-scattering measurements of the neutron Compton profile, $J(y)$ in polycrystalline ZrH_2 over a range of momentum transfers between 35 and 109 $Å^{-1}$. The measurements were performed using an inverse geometry spectrometer at a pulsed-spallation neutron source. The experimental results are compared with simulations calculated from a measurement of the density of states of the hydrogen vibrations in ZrH_2. Deviations from impulse approximation (IA) scattering and a form of the IA proposed by Stringari have been investigated. The deviations are manifest as both an asymmetry and a shift in centroid of $J(y)$. Both effects become less significant as the momentum transfer is increased and the IA limit is approached. At high momentum transfers the symmetrization procedure of Sears successfully removes final-state effects from these data. We conclude that the neutron Compton scattering technique can provide accurate information about the behavior of tightly bound proton systems such as ZrH_2.

I. INTRODUCTION

In recent years neutron Compton scattering (NCS) or deep inelastic neutron scattering (DINS) has become established as a technique for probing directly the momentum distribution of atoms in a variety of condensed matter systems. The technique was suggested by Hohenberg and Platzmann[1] almost 30 years ago and is analogous to the measurement of electron momentum by Compton scattering.[2] As with Compton scattering, the interpretation is based on the validity of the impulse approximation (IA) which is exact when both the energy and momentum transferred to the target atom are infinite.[3] Deviations of the dynamic scattering function from that derived under the IA occur at finite values of the momentum transfer **q**. Those arising as a consequence of the scattered neutron interacting with neighboring atoms are known as final-state effects (FSE's) while those arising from the bound state of the atom are known as initial-state effects (ISE's).[4] The question of when the IA may be deemed valid is still a matter of contention. A number of theories have been developed for calculating the form and magnitude of departures from the IA in helium[5–7] and Sears[8] has developed a treatment for FSE's which is applicable to a wide range of systems. It has been shown[9] that ISE's become significant at low temperatures and in quantum systems they are largely responsible for observed deviations from IA behavior. In nonquantum systems the IA is reached when the momentum transfer to the atom far exceeds the root-mean-square momentum of the atom. The derivation of the IA makes two assumptions. The first is that the momentum transfer is sufficiently large for the scattering to be incoherent and the second is that the struck atom gains sufficient energy from the neutron that its recoil appears to be that of a ''free'' atom. Deviations from the IA are usually attributed to FSE's but Stringari[10] pointed out that the standard form of the IA does not correctly treat the bound nature of the initial state. In this paper we examine the validity of the IA in zirconium hydride (ZrH_2) and test a form of the IA proposed by Stringari.

The NCS technique has already proved successful in determining atomic momentum distributions and in obtaining directly values for the mean atomic kinetic energies of a number of light elements, for example, solid[11,12] and liquid helium,[13,14] other noble gases in both solid and liquid phases,[15,16] hydrogen bonds,[17,18] metals,[19] liquid and solid hydrogen,[20] glasses,[21] and graphite.[22] Deviations from the IA are most significant at lower **q** where the spectrum of scattered neutrons does not exhibit the characteristic features expected for recoil scattering from a ''free'' target atom. For example, the determined momentum distribution is neither symmetric nor centered at zero momentum and interpretation follows the application of detailed correction procedures. Deviations from the IA are reduced by moving to larger **q** but they are not eliminated. Experiments on superfluid helium-4 performed with $\mathbf{q}>50$ $Å^{-1}$ still fail to observe the sharp signature expected for the Bose condensate fraction, showing that FSE's are still present.[23] Despite the theoretical interest in this subject experimental investigations are limited to helium and other noble gas systems.

High momentum transfers can be achieved with inverse-geometry spectrometers receiving electron-volt neutrons from pulsed-spallation neutron sources. Electron-volt spectroscopy is still in its infancy and as the reliability and accuracy of the technique improves the interpretation of results will become more reliant on the procedures used to correct for FSE's. Accurate measurements on tightly bound proton systems such as molecular hydrogen are only possible with electron-volt spectroscopy where energy transfers much greater than the vibrational frequency of the molecule are required before the IA can be reliably used to determine $n(\mathbf{p})$. A comprehensive assessment of the validity of the IA is essential if the NCS technique is to be routinely employed to investigate the momentum distribution of such tightly bound systems. Zirconium hydride was chosen for this investigation because (i) it is a strongly bound system, (ii) the incoherent neutron cross section of hydrogen is large at the very high momentum transfers used, (iii) its high Debye temperature ensures that the hydrogen is effectively in the ground state at room temperature, (iv) the harmonic approximation is valid and permits an exact calculation of $S_{\mathrm{IA}}(\mathbf{q},\omega)$ from a measurement of the vibrational density of states (DOS), and (v) the hydrogen and zirconium scattering are well separated by the kinematic mass separation of the NCS technique.

II. THEORETICAL BACKGROUND

A. Scattering within the impulse approximation

The double-differential scattering cross section for scattering from a system of N identical atoms at zero temperature is given by[24]

$$\frac{d^2\sigma}{d\Omega\ dE_1}=Nb^2\,\frac{|\mathbf{k}_i|}{|\mathbf{k}_f|}\,S(\mathbf{q},\omega), \tag{1}$$

where b is the scattering length, E_1 the energy of the scattered neutron, $\mathbf{k}_i$ and $\mathbf{k}_f$ are the initial and final neutron wave vectors, respectively, $\mathbf{q}$ is the neutron wave-vector transfer ($\mathbf{q}=\mathbf{k_i}-\mathbf{k_f}$), and $\hbar\omega$ is the energy lost by the neutron in the scattering process. The dynamic structure factor $S(\mathbf{q},\omega)$ can be written as

$$S(\mathbf{q},\omega)=\frac{1}{N}\sum_i g_i\left|\sum_n \langle i|\exp(-i\mathbf{q}\cdot\mathbf{r}_n)|f\rangle\right|^2\delta(\omega+E_i-E_f), \tag{2}$$

where $|i\rangle$ and $|f\rangle$ are the initial and final quantum states, $\mathbf{r}_n$ is the position coordinate of atom n, g_i is the Boltzmann factor for occupation of quantum state $|i\rangle$, and Σ_i performs a thermal average. The IA is reached in the limit of large wave-vector transfers where coherent processes are assumed minimal. Then incident neutrons scatter from individual nuclei independently and therefore respond only to a single-particle momentum distribution $n(\mathbf{p})$. The dynamical structure factor can then be written as

$$S_{\mathrm{IA}}(\mathbf{q},\omega)=\int_{-\infty}^{+\infty} n(p)\,\delta\!\left(\omega-\frac{(\mathbf{p}+\mathbf{q})^2}{2M}+\frac{p^2}{2M}\right)d\mathbf{p}, \tag{3}$$

where $S_{\mathrm{IA}}(\mathbf{q},\omega)$ is the dynamic scattering function in the IA, M is the atomic mass, and where $n(\mathbf{p})$ satisfies the normalization condition

$$\int_{-\infty}^{+\infty} n(\mathbf{p})d^3\mathbf{p}=1 \tag{4}$$

and the δ function restricts the integration to those states that are accessible with energy and momentum conservation. The average recoil energy transferred to the scattering particle is given by

$$\hbar\omega_R=\frac{\hbar^2q^2}{2M}. \tag{5}$$

Choosing $\mathbf{q}$ along the z axis of a Cartesian coordinate system gives

$$S_{\mathrm{IA}}(\mathbf{q},\omega)=\frac{M}{q}\,J(y), \tag{6}$$

where

$$y=\frac{M}{q}\left(\omega-\frac{q^2}{2M}\right) \tag{7}$$

and

$$J(y)=\int_{-\infty}^{\infty} n(p_x,p_y,y)dp_x\ dp_y. \tag{8}$$

The quantity $J(y)$ is often termed the "neutron Compton profile" (NCP), the one-dimensional projection of $n(\mathbf{p})$ along the direction of the scattering vector. The properties of $S(\mathbf{q},\omega)$ which follow from Eqs. (6)–(8) are known as y scaling and the degree to which the data obey this scaling law is a measure of the validity of the IA. For an isotropic momentum distribution it can be shown that

$$qS_{\mathrm{IA}}(\mathbf{q},\omega)=2\pi M\int_{|y|}^{\infty} pn(\mathbf{p})d\mathbf{p} \tag{9}$$

and the mean kinetic energy of the target particle, $\langle E_k\rangle$, may be determined from $J(y)$ from the second moment of the NCP,

$$\langle E_K\rangle=\frac{3}{2M}\int y^2J(y)dy. \tag{10}$$

B. The harmonic approximation

In the harmonic approximation, the atomic momentum distribution is identical to that of a free gas, except that the temperature is replaced by an effective temperature given by $\hbar^2\sigma^2=MT^*$ and Eq. (8) becomes

$$J(y)=\frac{1}{\sqrt{2\pi MT^*}}\exp\!\left(\frac{-y^2}{2MT^*}\right), \tag{11}$$

where T^* is the effective temperature defined by[4]

$$T^*=\frac{1}{2}\int \omega Z(\omega)\coth\!\left(\frac{\omega}{T}\right)d\omega \tag{12}$$

and $Z(\omega)$ is the phonon density of states. We define the variance of the momentum distribution along q as $\sigma=(MT^*)^{0.5}$. In this paper, energies and temperatures are measured in meV, momenta in Å^{-1} and masses in amu unless stated otherwise. In this system of units, $\hbar=2.044\,58$ Å meV$^{1/2}$ amu$^{1/2}$.

C. The Stringari formulation

The Stringari formulation[10] is obtained from the IA by replacing the $p^2/2M$ term with the mean kinetic energy $\langle E_k\rangle$ and the modified dynamical structure factor $S_s(\mathbf{q},\omega)$ is given by

$$S_s(q,\omega)=\int_{-\infty}^{\infty} n(p)\,\delta\!\left(\omega-\left(\frac{\mathbf{p}+\mathbf{q}}{2M}\right)^2+\langle E_k\rangle\right)d\mathbf{p}. \tag{13}$$

For an isotropic momentum distribution it can be shown that

$$qS_s(\mathbf{q},\omega)=2\pi M\int_{|y_1|}^{\infty} pn(\mathbf{p})d\mathbf{p}, \tag{14}$$

where

$$y_1=\sqrt{2M(\omega+\langle E_K\rangle)}-q \tag{15}$$

is the scaling variable, which should be compared with the IA scaling variable y given in Eq. (7). This predicts a negative shift of magnitude $\langle E_k\rangle$ in the peak energy of $S_s(\mathbf{q},\omega)$ from the IA value of $\hbar^2q^2/2M$.

D. Sears expansion

To account for deviations from the IA Sears[8] proposed a series expansion of $J(y)$ which contained symmetric and antisymmetric terms,

$$J_0(y)=J_{\mathrm{IA}}(y)-A_3\left[\frac{d^3J_{\mathrm{IA}}(y)}{dy^3}\right]+A_4\left[\frac{d^4J_{\mathrm{IA}}(y)}{dy^4}\right]-\cdots \tag{16}$$

where $J_0(y)$ is the observed NCP without instrument resolution and $J_{\mathrm{IA}}(y)$ is the NCS derived in the IA. The coefficients of the first symmetric and antisymmetric terms in the expansion are given by

$$A_3=\frac{M\langle\nabla^2V\rangle}{36\hbar^2q} \quad \text{and} \quad A_4=\frac{M^2\langle F^2\rangle}{72\hbar^4q^2}, \tag{17}$$

where V is the interatomic potential and $\langle F^2\rangle$ is the mean-squared force on the target atom during the scattering. The terms are corrections to the IA arising from FSE's and predict the magnitude and $\mathbf{q}$ dependence of deviations from the IA.

III. EXPERIMENTAL PROCEDURE

The measurements reported here were performed using the eVS at the ISIS facility, which is situated at the Rutherford Appleton Laboratory. The eVS is an inverse-geometry filtered-beam spectrometer which uses a foil with a strong cross section for neutron absorption to define the scattered neutron energy. A pulsed white beam of neutrons with energies in the range 1–100 eV is incident on the sample, and the time-of-flight (TOF) spectrum of the scattered beam is measured by an array of fixed detectors. A resonant foil difference technique is used to yield a set of TOF spectra for those neutrons scattered into a fixed energy and through fixed angles. A full description of the eVS can be found in the literature.[25]

At the time of the experiment reported here, the spectrometer had six banks of 10-atm ^{3}He neutron detectors arranged in pairs symmetrically about the incident beam and covering angles in the ranges 36°–54°, 57°–77°, and 125°–137°, respectively. The detectors were arranged with their axes vertical and centered at the beam height. Forty detectors were arranged at forward-scattering angles ($\theta<90°$) and a further ten at backward-scattering angles.[26] For scattering from hydrogenous systems the dynamics of the interaction restricts the scattering to scattering angles $\theta<90°$ and only data from detectors at forward scattering angles were useful in this investigation. Thirty of these were at angles suitable for hydrogen scattering and for convenience these are represented in this work as three banks—bank A (covering the angular range 36°–44°), bank B (46°–54°), and bank C (57°–66°). In Fig. 1 we show the TOF scans in $(\mathbf{q},\omega)$ space which were available with banks A, B, and C using a gold analyzer. The shaded region is bounded by the full width at half maximum (FWHM) of the response from a hydrogen atom in ZrH_2 (having a momentum distribution with a FWHM of 9 Å^{-1}). It should be noted that the energy and momentum transfers available on resonance filter spectrometers are much greater than those attainable on any other neutron instrument and it can be seen from Fig. 1 that on eVS, for H scattering at the recoil peak position, $2.5<\omega<23$ eV and $35<q<105$ Å^{-1}. At such high momentum and energy transfers, corrections to the IA are expected to be small, but as we shall show they are not negligible. The incident and transmitted beam intensities were monitored using glass scintillation detectors placed before and after the sample.

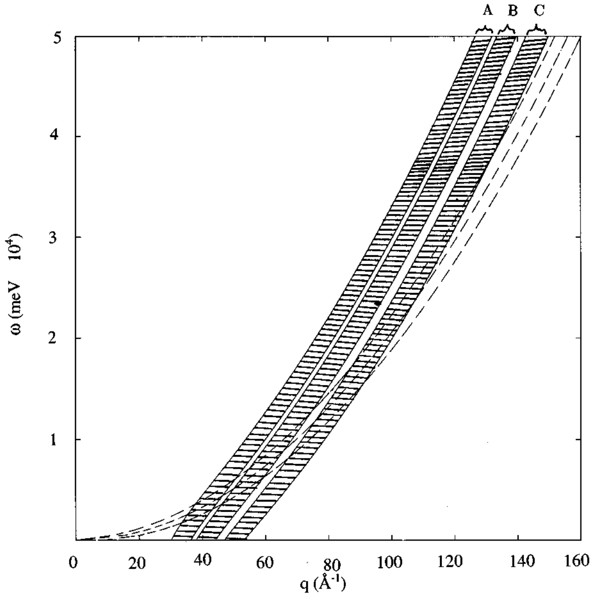

FIG. 1. Detector scans on eVS through $(\mathbf{q},\omega)$ space. In this work the eVS had 40 detectors at forward-scattering angles. 30 of these were at angles useful for hydrogen scattering, which are considered for convenience grouped together in three banks of detectors 36°–44° (bank A), 46°–54° (bank B), and 57°–66° (bank C). Each detector scan for each bank lies in the shaded region A, B, or C marked on the figure. The dashed curves represent the peak position and FWHM of the response of a hydrogen atom in ZrH_2 which has a momentum distribution with a FWHM of 9 Å^{-1}.

The sample was placed in a square aluminum can mounted on the end of an aluminum stick and positioned perpendicular to the beam. Detector saturation was avoided by limiting the total scattering to 5% of the incident beam. The beam tubes and the sample chamber were evacuated to minimize air scattering. The samples were manufactured at the Department of Physics of the University of Warwick from powdered samples of zirconium obtained from Goodfellow Metals (Cambridge). The grain size and purity of the powdered sample of zirconium were 150 μm and 99.50%, respectively. The percentage of hydrogen absorbed was carefully monitored during hydriding and the resulting composition was determined to be ZrH_x, $x=1.96\pm0.04$.

Gold foils were mounted on a cylindrical aluminum support which surrounded the sample chamber and placed in the scattered beam. The foils are automatically cycled in and out of the scattered beam every 5 min by means of pneumatic pistons. The constant cycling of the resonant foil minimizes systematic errors which result from changes in the relative efficiency of the detectors to neutrons of different energies. Two types of measurement were made: one with the resonant foils in and one with the resonant foils out of the scattered beam. The TOF spectra corresponding to the "foil in" and "foil out" measurements were collected in separate areas of the instrument computer memory. The gold foil has a strong absorption cross section of Lorentzian shape, centered at 4917.6 meV and with a half width at half maximum (HWHM) of 143.1 meV. By taking the difference between spectra collected with "foil in" and "foil out" the count rate for neutrons scattered with energy 4917.6±143.1 meV was determined.

The isotropic nature of the sample means that data from groups of detectors may be added together to increase the statistical accuracy. Summing data over banks of detectors with similar scattering angles results in a NCP of high statistical accuracy which covers a range of momentum transfer. Measurements were performed at both 20 and 290 K although the proton is effectively restricted to the ground state at both these temperatures. Furthermore, ZrH_2 exists in the ϵ phase at both these temperatures. This was confirmed by analysis of diffraction data which are recorded simultaneously with NCS data but in a different region of TOF (NCS 100–700 μs; diffraction 1000–20 000 μs). Diffraction peaks corresponding to d spacings greater than 1 Å were identified and the (002) peak due solely to the ϵ phase was observed.

Shown in Fig. 2 are typical TOF "foil out" and "foil in" spectra (each normalized to the incident beam) for scattering from ZrH_2 collected at a scattering angle of 36°. Shown in Fig. 3 is the difference of these two measurements for a series of detectors in one of the low-angle banks. The difference spectrum yields those neutrons absorbed by the analyzer foil. The broad peak is the hydrogen scattering, while the narrow peak is the combined scattering from the zirconium and the aluminum sample holder. Note how the separation of the two peaks and the width of the hydrogen peak become larger at higher scattering angles.

IV. ANALYSIS

The data analysis procedures for the eVS are described fully elsewhere[25] and only a summary is given here. The "foil in" and "foil out" TOF spectra obtained by each detector were suitably normalized and then subtracted. The aluminum can scattering was determined by an empty can measurement and then subtracted from the data. The zirconium scattering was removed by fitting an appropriate Voigt function (convolution of a Gaussian and a Lorentzian) to each TOF data set, the parameters of the Voigt function being determined by the instrument resolution and the Gaussian width of the zirconium recoil scattering. The TOF spectrum from each detector was then transformed into y space using either the IA or the Stringari scaling expressions, Eqs. (7) and (15), respectively.

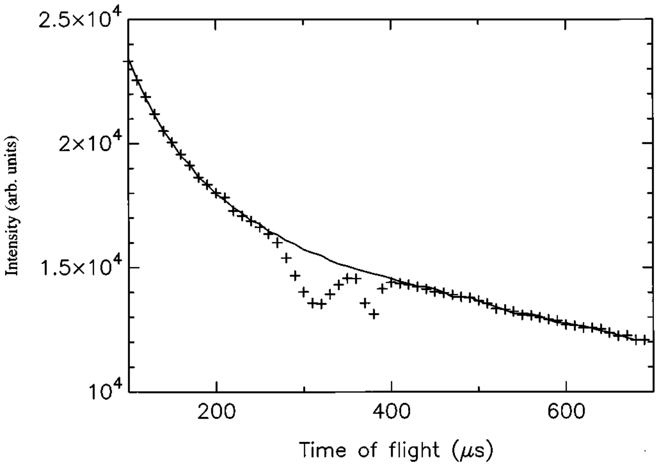

FIG. 2. Foil in (crosses) and foil out (line) time-of-flight measurements of ZrH_2 on eVS. The scattering angle for these measurements was 36°.

Analytical expressions for the components of the instrument resolution function in y space[27] were used to calculate the resolution components and the results for detector bank C are given in Fig. 4. The contributions are independent and originate from the distribution of the initial and final flight paths (σ_0 and σ_1, respectively), and scattering angles and incident energy values allowed by the instrument geometry, σ_θ, and the analyzer foil, σ_E. In all cases the dominant contribution is σ_E although the angular term σ_θ is significant for scattering from hydrogenous systems and was determined for all detectors from the line shape of powder diffraction peaks. The intrinsic energy width of the gold resonance was previously determined for each detector, both analytically and experimentally by measurements of recoil scattering from heavy systems such as lead and tin, and is well described by a Lorentzian function. All other resolution components are well described by Gaussian functions. The resultant resolution function is therefore a Voigt function.

The mean atomic kinetic energy was determined by fitting each individual momentum-space difference spectrum with a Gaussian, of the form given in Eq. (18) below, convoluted with the appropriate resolution function

$$J(y)=\left(\frac{1}{\sqrt{2\pi\sigma_y^2}}\right)\exp\left(\frac{-(y-y_m)^2}{2\sigma_y^2}\right). \tag{18}$$

Two fitting parameters were used; the profile centroid y_m and standard deviation σ_y. The mean atomic kinetic energy was determined from the value of σ_y whereas deviations of y_m from zero were used to test the validity of the IA and to investigate the significance of FSE's. Values of σ_y were averaged to give a single value for each detector bank. These values were further averaged and used to determine the Debye-Waller factor used to calculate the density of states.

V. DENSITY OF STATES

As mentioned in Sec. II, exact simulations of $J(y)$ can be performed by calculating the scattering function $S(\mathbf{q},\omega)$ for an isotropic harmonic solid using the density of states. Although ϵ-phase ZrH_2 has been studied in great detail, we

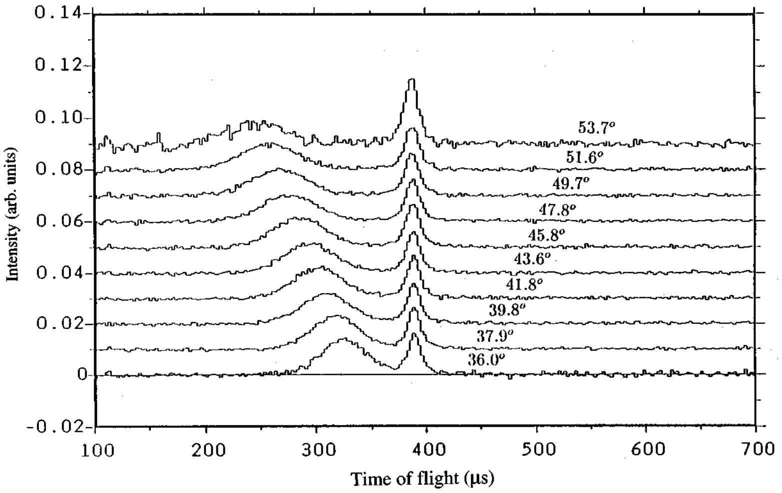

FIG. 3. A series of time-of-flight difference measurements of ZrH_2 measured on one of the low-angle detector banks on eVS. The broad peak is scattering from hydrogen, while the narrow peak is scattering from aluminum (in the sample holder) and zirconium. Note how the separation of the two peaks and the width of the hydrogen peak both become larger at high scattering angles.

know of no previous attempt to derive the phonon density of states explicitly. The theoretical results required for our analysis are detailed below.

An exact calculation of both the single-particle $S(\mathbf{q},\omega)$ and $n(\mathbf{p})$ from the density of states is possible within the harmonic approximation.[28] For an isotropic system, the single-particle incoherent scattering in the harmonic approximation is given by[24]

$$S_H(\mathbf{q},\omega)=\left[\frac{1}{2\pi\hbar}\right]\int_{-\infty}^{\infty} dt\ \exp(-i\omega t)\exp\left(\frac{\hbar^2 q^2}{2M}\right.$$
$$\left.\times[\gamma(t)-\gamma(0)]\right], \qquad (19)$$

where

$$\gamma(t)=\int_{-\infty}^{\infty} d\omega[Z(\omega)/\omega]n(\omega)\exp(-i\omega t). \qquad (20)$$

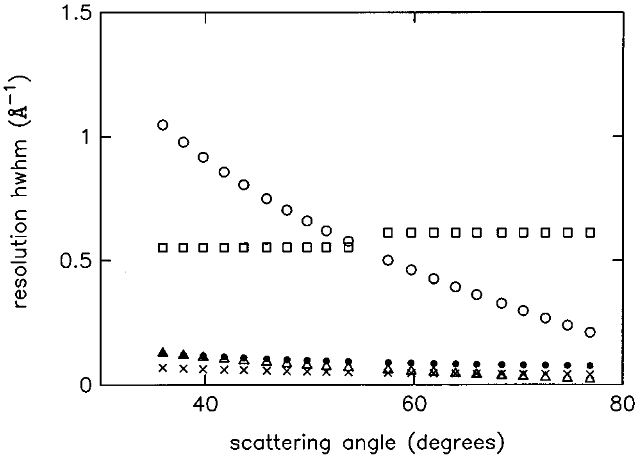

FIG. 4. Calculated resolution components of eVS for hydrogen scattering over all forward-scattering detectors (banks *A*, *B*, and *C*) obtained from separate measurements on heavy elements. The different resolution components arise from the analyzer foil, σ_E (open circles), the scattering geometry, σ_θ (squares), the uncertainty of the measurement in time of flight (crosses), and the distribution of the initial and final flight paths, σ_0 (open triangles) and σ_1 (solid circles), respectively.

The one-phonon contribution to $S_H(\mathbf{q},\omega)$ can be obtained from (19) by expanding the exponential term $\exp(-i\omega t)$ and is given by

$$S_{H,+1}(\mathbf{q},\omega)=\frac{1}{2M}q^2\exp[-2W(\mathbf{q})]\left[\frac{Z(\omega)}{\omega}\right][n(\omega)+1], \qquad (21)$$

where the subscript $+1$ refers to phonon creation, $Z(\omega)$ is the normalized phonon density of states, $W(q)$ is the Debye-Waller factor, and $n(\omega)$ is the Bose-Einstein occupation factor $n(\omega)=[\exp(\hbar\omega/k_BT)]^{-1}$ where k_B is Boltzmann's constant. At low $\mathbf{q}$, $S(\mathbf{q},\omega)$ is dominated by one-phonon scattering and the density of states can be derived directly from Eq. (21). Following the method used by Andreani[29] for a polycrystalline sample the density of states $g(\omega)$ is given by

$$g(\omega)=\lim_{q\to 0} g'(\mathbf{q},\omega)=\frac{S_{H,+1}(\mathbf{q},\omega)}{q^2}2M\omega\frac{\exp 2W(\mathbf{q})}{[n(\omega)+1]}. \qquad (22)$$

For a cubic Bravais lattice $W(\mathbf{q})=q^2/2\sigma^2$ and if $W(\mathbf{q})$ is known $g(\omega)$ can be calculated from a measurement of $S(\mathbf{q},\omega)$. $W(\mathbf{q})$ was determined using a value of $\sigma=4.18$ Å^{-1} and $S(\mathbf{q},\omega)$ was measured using the MARI spectrometer at ISIS. A complete account of the experimental procedure and a discussion of the MARI results will be given elsewhere[30] and only a brief description is included here.

MARI is a direct-geometry chopper spectrometer operating in TOF.[31] It has a very large array of neutron detectors distributed over a wide range of angles which allow $S(\mathbf{q},\omega)$ to be measured over a range of values in $(\mathbf{q},\omega)$ space with a resolution that is typically 1–2 % of the incident energy. The energy of the incident pulses of neutrons is determined by the rotational speed of the Fermi chopper, phased to the neutron burst time. This energy sets the maximum energy of the region of $(\mathbf{q},\omega)$ space to be observed. The maximum momentum transfer available on MARI for scattering from hydrogenous samples is about 20 Å^{-1}, compared to about 100 Å^{-1} for eVS.

Multiple-scattering effects were investigated by performing three experiments, all at 20 K with two different sample geometries and two different incident energies (220 and 450

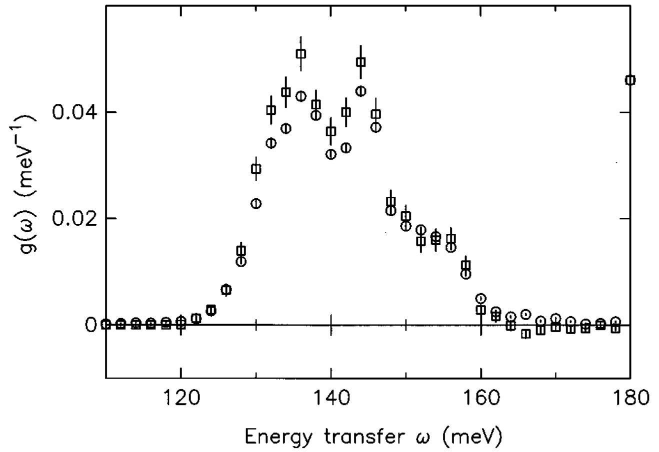

FIG. 5. The vibrational density of states of H in ZrH_2 obtained from the measurement of $S(\mathbf{q},\omega)$ with a slab sample geometry (circles) and that obtained with a cylindrical sample geometry (boxes). Both runs were made with an incident energy of 220 meV. The similarity of the derived density of states for these two different geometries indicates that multiple-scattering effects are small.

meV). To minimize systematic errors in the derived density of states it is important to ensure that multiple scattering does not adversely affect the data at low **q**. In each measurement the scattered intensity was of the order of 5%, low enough to ensure that multiple scattering was not significant. If significant, the different combinations of sample geometry and incident energy would yield significantly different results for the derived vibrational density of states. This was not the case. There is the advantage that the exact form of the vibrational density of states does not affect the form of the NCP at large **q**. The width of the NCP should only depend on the mean kinetic energy of the system, and therefore on the density of states via the effective temperature, Eq. (12).

The MARI data were in the form of a rectangular grid of values of $S(\mathbf{q},\omega)$. A series of constant-ω cuts were made at intervals of between 0.5 and 1.0 meV. Each of the data sets so obtained was converted to a value defined here as $g'(\omega,\mathbf{q})$. By extrapolating $g'(\omega,\mathbf{q})$ to $\mathbf{q}=0$ for each value of ω, and normalizing to unity, $g(\omega)$ was obtained. A weighted least-squares straight-line fit was used to perform the extrapolation. Once the extrapolated values were obtained in the region 100–200 meV, they were normalized to unity. Figure 5 shows the derived density of states, corresponding to MARI data obtained with an incident energy of 220 meV and slab and cylindrical sample geometries (circles and boxes respectively). The density of states obtained with the higher incident energy was of poorer resolution and is not shown.

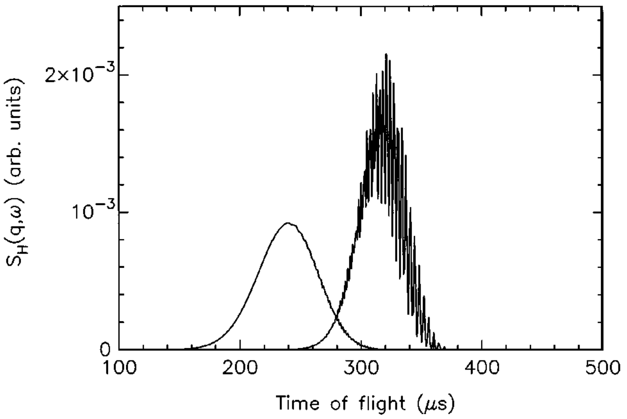

FIG. 6. Simulations of eVS time-of-flight spectra for scattering from hydrogen in ZrH_2. The simulations are based on the measurement of the vibrational density of states (incident energy 220 meV) and are an exact numerical simulation in the harmonic incoherent approximation. The simulations shown are for detectors at scattering angles of 36.0° and 53.7°. The individual multiphonon excitations are visible in the peak centered at about 310 μs. At the higher momentum transfers reached at 53.7°, the individual excitations merge together. The data shown are not resolution convoluted.

VI. EXPERIMENTAL RESULTS AND SIMULATIONS

Simulations of the measured neutron Compton profiles of ZrH_2 in TOF were performed using the density of states shown in Fig. 5 as boxes (see Ref. 9). The slab geometry measurement had the best counting statistics and this density of states was used to simulate eVS data. Data were simulated using the calibration parameters appropriate to each of the 30 detectors used in the measurements. Three profiles were created by adding simulated data corresponding to detectors in each of the three detector banks A, B, and C. The simulated TOF spectra were convolved with the resolution function for each detector, converted to momentum space, and then analyzed in the same way as the "real" eVS data. A value of 143.1 meV was used for the full width at half maximum of the Lorentzian resolution contribution from the analyzer foil. Simulations in TOF for scattering angles of 35.96° and 53.68° are shown in Fig. 6 before convolution with the instrument resolution. The individual multiphonon excitations are visible. Higher momentum transfers are reached at the larger scattering angle of 53.68° and the individual excitations merge together. After convolution with the resolution function there was no sign of the individual excitations for even the lowest scattering angle (lowest momentum transfer).

The results of the simulations of the measured NCP for detector banks A, B, and C are compared to eVS measurements in Figs. 7(a), 7(b), and 7(c). The y scaling procedure [Eq. (7)] was used to convert the TOF data to momentum space. The profiles measured by each of the ten detectors in each bank have been summed and normalized to unity. The momentum transfer ranges sampled by banks A, B, and C were 35.3–46.6 Å^{-1}, 50.0–65.8 Å^{-1}, and 75.7 and 108.6 Å^{-1}, respectively. The simulations based on the measured vibrational density of states are shown as solid lines. Shown also is the sum of four measurements of hydrogen in ZrH_2. Three of these measurements were the results of a previously unpublished experiment on a commercially supplied sample of ZrH_2 (Ref. 32) and the other used the sample prepared for the density of states measurement. Good experimental consistency is observed. The difference between the simulation and the IA result calculated directly from the density of states is shown as the lower solid line. In both the simulation and the eVS data an asymmetry is observed. As expected, at finite values of **q**, the peak position is shifted to negative values of momentum space. Both the asymmetry and peak

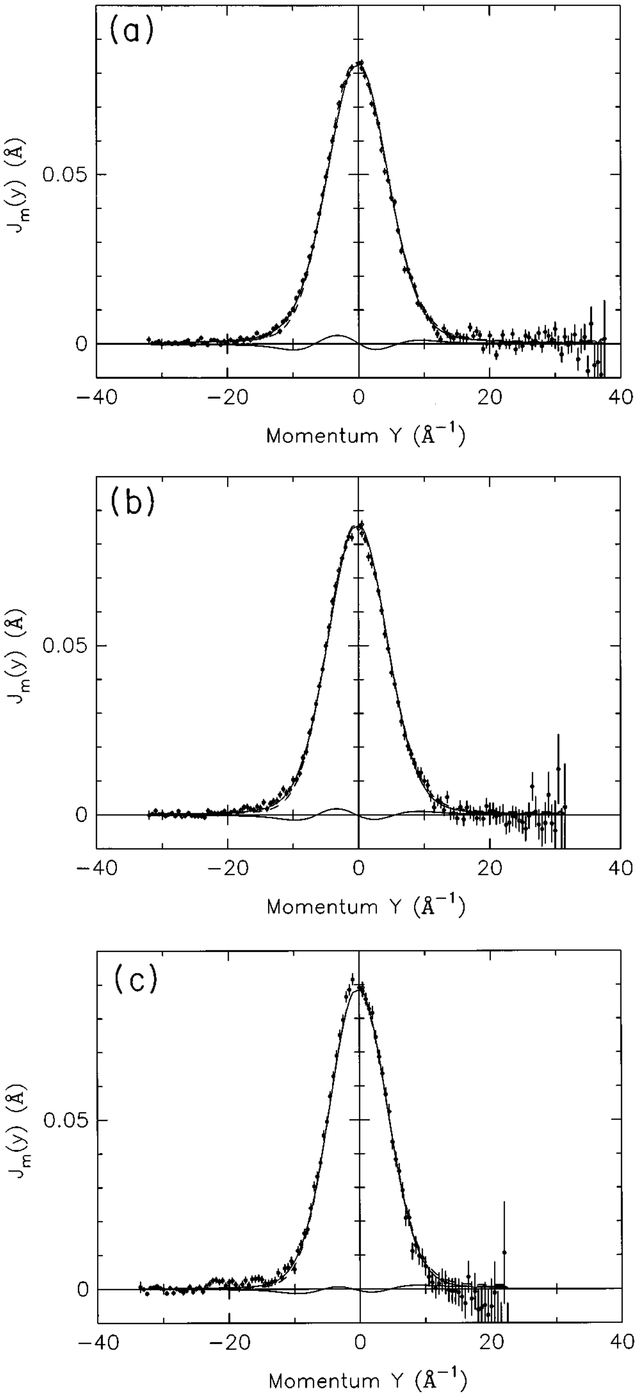

FIG. 7. Comparison of measurements of $J_m(y)$ made at average momentum transfers of (a) 40.8 Å^{-1} (bank *A*), (b) 57.6 Å^{-1} (bank *B*), and (c) 91.2 Å^{-1} (bank *C*), respectively, on eVS (+) compared to exact simulations of the data based on the density of states of the hydrogen vibrations measured with the MARI spectrometer (solid line). The form of $J_m(y)$ reached in the impulse approximation is also shown (dashed line). The difference between this and the simulation is shown as the lower solid line. The conventional y scaling was used to transform from time of flight to momentum space.

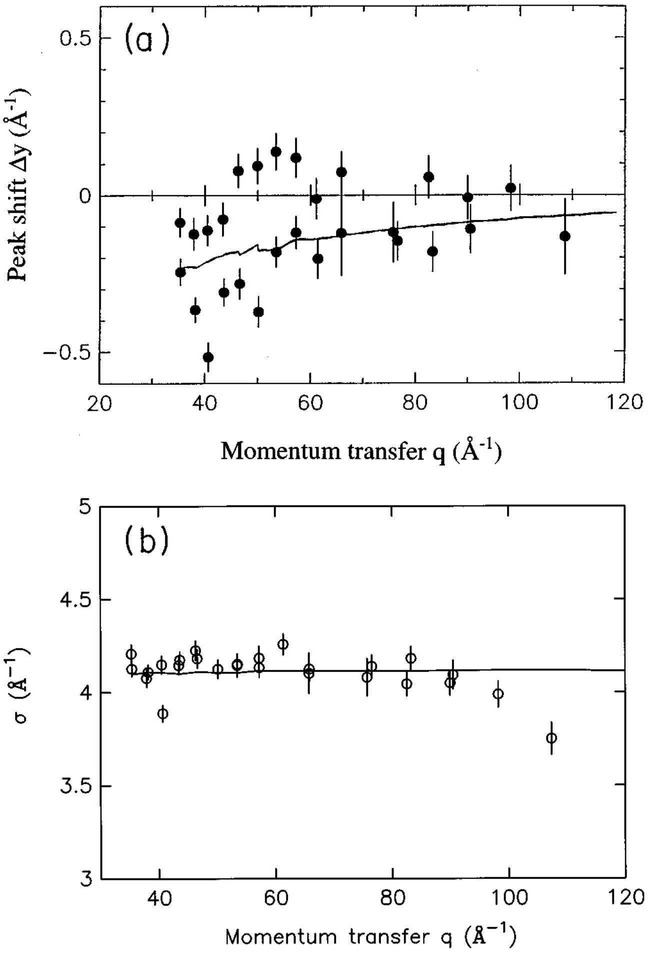

FIG. 8. (a) The positions of the recoil peaks in y space are shown for the eVS measurements (circles) as a function of the momentum transfer of the measurements. Also shown (solid line) is the same for the numerical simulation. (b) The σ values determined from the eVS measurements (circles). They are plotted against the σ values determined from the numerical simulation from the vibrational density of states (solid line).

shift are attributed to the presence of FSE's. To demonstrate the approach to the IA as **q** increases, the measured peak position of each profile was determined. The peak position was not affected by the resolution function as this is symmetric. Figure 8(a) shows the peak shifts in the y scaled eVS data and the derived peak shifts of the simulated data plotted as a function of y. The peak positions as a function of y are also shown for the simulated data. The peak shifts become progressively smaller as the momentum transfer is increased, in accordance with the limiting behavior of the IA. This observation is reinforced by returning to Fig. 7 where the difference between the IA and simulation is reduced as the momentum transfer is increased from banks *A* to *C*.

Figure 9 corresponds to Fig. 7 except that the Stringari y_1 scaling variable has been used to convert from TOF to momentum space. The difference is clear. The measured neutron Compton profiles are distinctly more asymmetric than the y-transformed data.

The mean atomic kinetic energy $\langle E_k \rangle$ can be deduced by fitting with a model having the form of Eq. (18) and using $\langle E_k \rangle = 3\sigma_y{}^2/2M$. Figure 8(b) shows the fitted values of σ_y as a function of y for the eVS data (circles) and the results obtained from the simulation (solid line). The dependence of σ_y on the form of the density of states was tested by repeating the simulations for ZrH_2 using a slightly different density of states and with σ_y values of 4.14 and 4.17 Å^{-1}, respec-

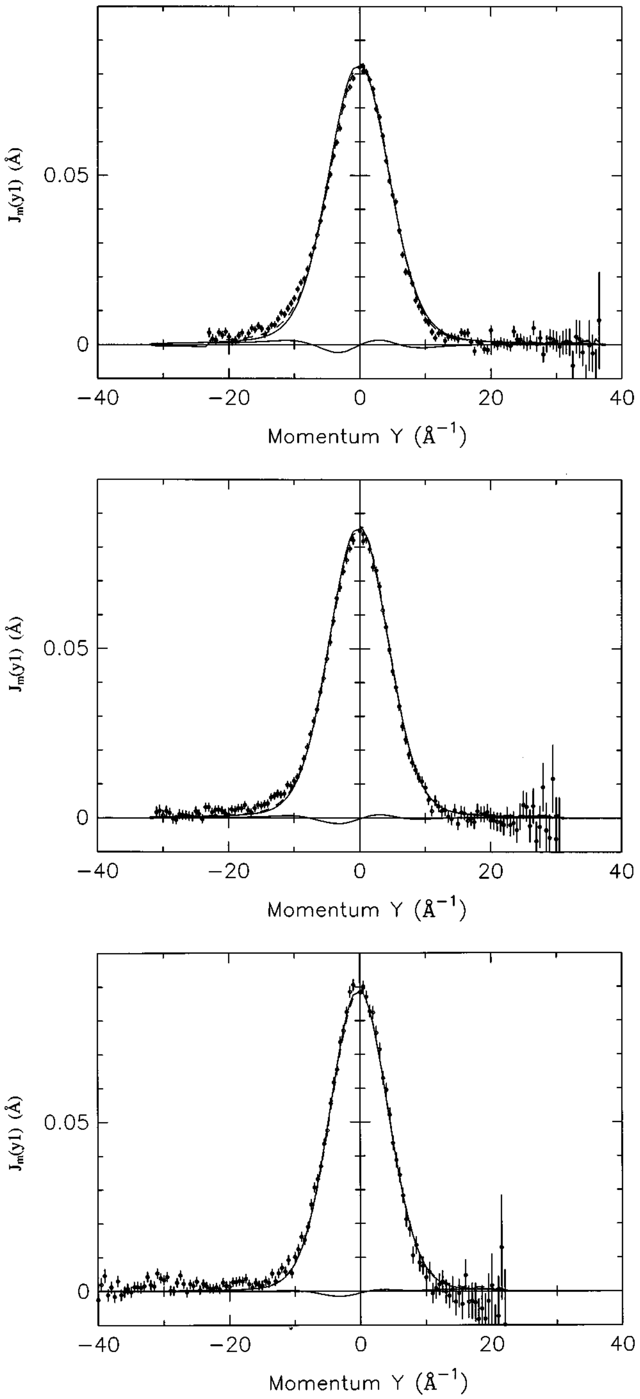

FIG. 9. This is the analogous diagram to Fig. 7 except in this case y_1 scaling was used to convert from time of flight to momentum space.

tively. The values extracted from the two simulated profiles were 4.123±0.002 and 4.141±0.002 Å^{-1}. The difference in these values (1%) indicates the sensitivity of the derived value to the mean value of the density of states used in the simulations. However, the form of the density of states has little bearing on the simulations. After applying the Sears symmetrization procedure outlined in Sec. II the symmetrized y-transformed simulation gave a value of σ=4.154 Å^{-1}, which agrees well with the value of 4.14 Å^{-1} derived from the density of states.

The sensitivity of σ_y to the half width at half maximum of the Lorentzian contribution to the resolution function was determined by repeating the y-transformed simulations using values of ΔE_R=126 and 143.1 meV. For the hydrogen simulations, the two analyses gave values of 4.146±0.002 and 4.123±0.002 Å^{-1}, respectively, a difference of about 0.75% or just under 1.44% in the mean kinetic energy. This is comparable to the statistical accuracy of the measurement, and so is not of great significance. This justified the value of ΔE_R=140 meV used consistently in the analysis.

Table I gives σ_y determined from the density of states directly, through Eq. (12) (the harmonic approximation), from the symmetrized and unsymmetrized neutron Compton profiles simulated from the density of states, and from the symmetrized and unsymmetrized measured neutron Compton profiles. Values obtained using both y and y_1 scaling are given for the simulated and measured data. The Stringari IA (SIA) transformation generally leads to an overestimation of the mean kinetic energy compared with that calculated directly from the density of states. This is consistent with the asymmetry observed in Fig. 9. FSE's also result in a profile asymmetry which can be corrected by symmetrization of $J(y)$. This procedure removes FSE's of order $\mathbf{q}^{-1}$ and is applicable to these data because FSE's are expected to be small at the high momentum transfers used. The values for σ_y thus obtained are typically 1% larger than the unsymmetrized values. For the symmetrized y-transformed simulations, the results agree within error with the value of 4.14 Å^{-1} calculated directly from the density of states. The values measured at the low and intermediate momentum transfer (banks *A* and *B*) are also in agreement. The small underestimation at higher $\mathbf{q}$ (bank *C*) may be attributed to a systematic error resulting from instability in the measurement at very short times of flight.

VII. CONCLUSIONS

We have used neutron Compton scattering from ZrH_2 to test the validity of the IA and SIA in scattering from hydrogenous systems. We find that using the Stringari scaling variable y_1 introduces a significant asymmetry in $J(y_1)$ and the extracted kinetic energy is significantly larger (2%) than the value determined from the density of states directly. Our data suggest that y scaling is more appropriate for tightly bound hydrogenous systems such as ZrH_2. FSE's are manifested in our data by shifts in the peak position to negative y values and as a profile asymmetry. Both effects are reduced at high $\mathbf{q}$ as the IA is approached. For $\mathbf{q}>40$ Å^{-1} symmetrization removes FSE's to the accuracy of these data. At lower $\mathbf{q}$ we believe effects of order $\mathbf{q}^{-2}$ remain. We conclude that electron-volt spectroscopy with the energy and momentum transfers currently available can be used to obtain accurate results on tightly bound hydrogenous systems.

It is perhaps not surprising that the y_1 scaling is inaccurate in zirconium hydride. It has been shown[9] that y_1 scaling is a preferable description to y scaling in an infinite square-well potential. In this case, the energy of the particle is entirely kinetic and the replacement of the initial energy by the kinetic energy E_k is exact. Stringari also showed that y_1 scaling provides an accurate description of deviations from the

TABLE I. The variance σ_y of $J(y)$ (unsymmetrized) of hydrogen in ZrH_2 determined from exact numerical calculations described in the text (σ_{sim}) and measurements made on the eVS spectrometer (σ_m) for three ranges of momentum transfer. The results of the symmetrized calculations and measurements are also given ($\sigma_{S\text{sim}}, \sigma_{Sm}$). Values are compared to σ_{DOS} determined from the density of states directly through Eq. (12). The numbers in parentheses are the errors.

Profile widths (Å^{-1})	Bank *A* q_{mean}=40.8 Å^{-1}		Bank *B* q_{mean}=57.6 Å^{-1}		Bank *C* q_{mean}=91.2 Å^{-1}	
Scaling variable	y[a]	y_1[a]	y	y_1	y	y_1
σ_{sim}	4.106(0.007)	4.149(0.008)	4.112(0.005)	4.159(0.005)	4.117(0.005)	4.165(0.005)
$\sigma_{S\text{sim}}$	4.151(0.005)	4.149(0.006)	4.160(0.004)	4.169(0.004)	4.169(0.003)	4.192(0.003)
σ_m	4.12(0.01)	4.17(0.02)	4.16(0.02)	4.21(0.02)	4.03(0.06)	4.06(0.03)
σ_{Sm}	4.15(0.01)	4.20(0.01)	4.17(0.01)	4.21(0.01)	4.03(0.02)	4.09(0.02)
σ_{DOS}	4.14		4.14		4.14	

[a] y and y_1 scaling variables are described in the text.

impulse approximation in liquid helium. The interatomic potential in liquid helium is similar to the square-well potential in that it is weak, except at short interatomic distances. The effect of a longer-range interatomic potential, such as the harmonic potential in zirconium hydride, is to reduce shifts in the peak position of $J(y)$, compared with the predictions of y_1 scaling. Thus the type of scaling which is observed will depend on the nature of the interatomic potential.

ACKNOWLEDGMENTS

This research was supported in part by the U.K. Science and Engineering Research Council under Contract Nos. GR/H97161 and GR/H03919. We are grateful to the SERC for the provision of beamtime and research support at the ISIS neutron factility. The ZrH_2 sample was manufactured at the University of Warwick with the assistance of Dr. G. Styles.

---

*Present address: Rutherford Appleton Laboratory, Chilton, Didcot, Oxfordshire OX11 0QX, UK.

[1] P. C. Hohenberg and P. M. Platzmann, Phys. Rev. **152**, 198 (1966).

[2] *Compton Scattering*, edited by B. Williams (McGraw-Hill, New York, 1977).

[3] V. F. Sears, Phys. Rev. A **5**, 452 (1971); **7**, 340 (1973); J. J. Weinstein and J. W. Negele, Phys. Rev. Lett. **49**, 1016 (1982).

[4] J. Mayers, C. Andreani, and G. Baciocco, Phys. Rev. B **39**, 2022 (1989).

[5] C. Carraro and S. E. Koonin, Phys. Rev. Lett. **65**, 2792 (1990).

[6] A. Belic and V. R. Pandharipande, Phys. Rev. B. **45**, 839 (1992).

[7] R. N. Silver, Phys. Rev. B **37**, 3794 (1988); **38**, 2283 (1988); **39**, 4022 (1989).

[8] V. F. Sears, Phys. Rev. B **30**, 44 (1984).

[9] J. Mayers, Phys. Rev. B **41**, 41 (1990).

[10] S. Stringari, Phys. Rev. B **35**, 2038 (1987).

[11] R. O. Hilleke, P. Chaddah, R. O. Simmons, D. L. Price, and S. K. Sinha, Phys. Rev. Lett. **52**, 847 (1984).

[12] R. C. Bladsdell, D. M. Ceperley, and R. O. Simmons, Z. Naturforsch. Teil A **48**, 433 (1993).

[13] H. Mook, Phys. Rev. B **37**, 5806 (1988); W. M. Snow, Y. Yang, and P. E. Sokol, Europhys. Lett. **19**, 403 (1992).

[14] K. H. Anderson, W. G. Stirling, A. D. Taylor, S. M. Bennington, Z. A. Bowden, I. Bailey, and H. R. Glyde, Physica B **181**, 865 (1992).

[15] D. A. Peek, I. Fujita, M. C. Schmidt, and R. O. Simmons, Phys. Rev. B **45**, 9680 (1992); M. A. Fradkin, S. X. Zeng, and R. O. Simmons, *ibid.* **49**, 3197 (1994); D. N. Timms, A. C. Evans, J. Mayers, M. Boninsegni, D. M. Ceperley, and R. O. Simmons (unpublished).

[16] D. A. Peek, M. C. Schmidt, I. Fujita, and R. O. Simmons, Phys. Rev. B **45**, 9671 (1992).

[17] P. Postorino, F. Fillaux, J. Mayers, J. Tomkinson, and R. S. Holt, J. Chem. Phys. **94**, 4411 (1991).

[18] J. Noreland (private communication).

[19] A. C. Evans, J. Mayers, D. N. Timms, and M. J. Cooper, Z. Naturforsch. Teil A **48**, 425 (1993); S. Fulton, R. A. Cowley, and A. C. Evans, J. Phys. Condens. Matter **6**, 2977 (1994); A. C. Evans, J. Mayers, and D. N. Timms, *ibid.* **6**, 4197–4212 (1994).

[20] W. E. Langel, D. L. Price, R. O. Simmons, and P. E. Sokol, Phys. Rev. B **38**, 275 (1988); K. W. Herwig, J. C. Gavilano, M. C. Schmidt, and R. O. Simmons, *ibid.* **41**, 96 (1990); J. Mayers, Phys. Rev. Lett. **71**, 1553 (1993).

[21] F. J. Bermejo, F. J. Mompeán, A. Srinivasan, J. Mayers, and A. C. Evans, Phys. Lett. A **189**, 333 (1994).

[22] M. P. Pauli and R. S. Holt, J. Phys. C **21**, 3633 (1988); H. Rauh and N. Watanabe, Phys. Lett. **100A**, 244 (1984).

[23] R. S. Holt, L. M. Needham, and M. P. Pauli, Phys. Lett. **126**, 373 (1987).

[24] S. W. Lovesey, *Theory of Neutron Scattering from Condensed Matter* (Oxford University Press, New York, 1987).

[25] J. Mayers and A. C. Evans (unpublished).

[26] For an example of a typical setup, see A. C. Evans, J. Mayers, and D. N. Timms, J. Phys. Condens. Matter **6**, 4197 (1994).

[27] C. Andreani, G. Baciocco, R. S. Holt, and J. Mayers, Nucl. Instrum. Methods Phys. Res. Sect. A **276**, 297 (1989).

[28] J. M. F. Gunn, C. Andreani, and J. Mayers, J. Phys. C **19**, L835 (1986).

[29] C. Adreani, Mol. Phys. **73**, 737 (1991).

[30] A. C. Evans, D. N. Timms, J. Mayers, and S. M. Bennington (unpublished).

[31] S. M. Bennington and R. S. Eccleston (unpublished).

[32] A. C. Evans (private communication).